

## Hartree-Fock Ground State Phase Diagram of Jellium

L. Baguet,<sup>1</sup> F. Delyon,<sup>2</sup> B. Bernu,<sup>1,\*</sup> and M. Holzmann<sup>1,3</sup>

<sup>1</sup>LPTMC, UMR 7600 of CNRS, Université Pierre et Marie Curie, F-75252 Paris Cedex 05, France

<sup>2</sup>CPHT, UMR 7644 of CNRS, École Polytechnique, F-91128 Palaiseau Cedex, France

<sup>3</sup>Université Grenoble 1/CNRS, LPMMC UMR 5493, Maison des Magistères, 38042 Grenoble, France

(Received 11 July 2013; published 14 October 2013)

We calculate the ground state phase diagram of the homogeneous electron gas in three dimensions within the Hartree-Fock approximation and show that broken symmetry states are energetically favored at any density against the homogeneous Fermi gas state with isotropic Fermi surface. At high density, we find metallic spin-unpolarized solutions where electronic charge and spin density form an incommensurate crystal having more crystal sites than electrons. For  $r_s \rightarrow 0$ , our solutions approach pure spin-density waves, whereas the commensurate Wigner crystal is favored at lower densities,  $r_s \gtrsim 3.4$ . Decreasing the density, the system undergoes several structural phase transitions with different lattice symmetries. The polarization transition occurs around  $r_s \approx 8.5$ .

DOI: [10.1103/PhysRevLett.111.166402](https://doi.org/10.1103/PhysRevLett.111.166402)

PACS numbers: 71.10.Ca, 71.10.Hf, 71.30.+h

The understanding of electrons in solid state and condensed matter has been one of the major challenges since the discovery of quantum mechanics. The simplest model system representing condensed matter is the homogeneous electron gas (jellium) where electrons interact with each other and with a uniform positive charged background density  $3/(4\pi a_B^3 r_s^3)$  instead of the nuclei, where  $a_B$  is the Bohr radius. For almost a century, jellium has been the central model for qualitative and quantitative studies of electronic correlation [1–10].

The Hartree-Fock (HF) approximation plays an absolutely fundamental role in tackling many-body electron problems. As the best possible description within the independent particle approximation, it provides both a reference and a starting point for any more sophisticated calculations. However, even though the HF ground state of jellium has been the subject of research over the years [10–12], the ground state phase diagram as a function of the density has still not fully been established. At low density, potential energy largely dominates over the kinetic energy, and the electrons form the so-called Wigner crystal (WC), the ground state in the classical limit, whereas in the limit of vanishing  $r_s$  the ideal Fermi gas (FG) is approached. Overhauser has argued that the FG solution never represents the true HF ground state at any finite density [10]. Only quite recently, indications for a ground state with broken spin symmetry in the high density region were found in explicit numerical calculations for small and moderate sizes [12]. However, its energy gain compared to FG has not been established in the thermodynamic limit.

Here, we present the Hartree-Fock phase diagram covering relevant crystal structures [13]. Generalizing previous approaches to form charge and spin broken symmetry states [10,12], our study also includes the possibility of incommensurate crystals of charge and spin density. In contrast to WC states, the number of maxima of the charge

and spin density there differs from the number of electrons, thus providing broken symmetry states with metallic character [14,15]. At high densities, we find that these incommensurate states are favored against FG and WC leading to spin density waves (SDW). Our method allows us to treat large enough systems to obtain results valid in the thermodynamic limit, necessary to clearly establish the tiny gain of energy for these states. Our study also suggest new candidate ground states for jellium and jelliumlike systems [16] that should be explored by more accurate many-body approaches [1,9].

We consider a system of  $N$  electrons in a volume  $V$ , embedded in an homogeneous background of opposite charge, interacting through the Coulomb potential using periodic boundary conditions. Hartree-Fock solutions are Slater determinants  $|\Psi\rangle = \Lambda_{\alpha \in S} |\phi_\alpha\rangle$  constituted by a set  $S$  of single-particle states  $\phi_\alpha$ . The Hartree-Fock solutions can be defined by a one-body density matrix  $\rho_1$  such that  $\text{Tr}\rho_1 = 1$  and  $0 \leq \rho_1 \leq 1/N$ . The two-body density matrix  $\rho_2$  satisfies

$$\rho_2(\underline{1}, \underline{2}; \underline{1}', \underline{2}') = \rho_1(\underline{1}; \underline{1}')\rho_1(\underline{2}; \underline{2}') - \rho_1(\underline{1}; \underline{2}')\rho_1(\underline{2}; \underline{1}'). \quad (1)$$

Now we restrict our study to periodic states. Let  $\Lambda^*$  be the lattice generated by  $\mathbf{L}_1, \mathbf{L}_2, \mathbf{L}_3$ . Our periodic simulation box is a parallelepiped of sizes  $M\mathbf{L}_i$ , for some integer  $M$ , and volume  $V \sim M^3$ , where we assume  $\rho_1(\mathbf{r} + \mathbf{L}_i, \mathbf{r}' + \mathbf{L}_i) = \rho_1(\mathbf{r}, \mathbf{r}')$ . The reciprocal lattice  $\Lambda$  is generated by  $\mathbf{Q}_1, \mathbf{Q}_2$ , and  $\mathbf{Q}_3$  ( $\mathbf{L}_i \cdot \mathbf{Q}_j = 2\pi\delta_{ij}$ ), and  $\rho_1$  can be written as

$$(\rho_1 \psi)(\mathbf{k} + \mathbf{q}, \sigma) = \sum_{\mathbf{q}' \in \Lambda, \sigma'} \rho_{\mathbf{k}}(\mathbf{q}, \sigma; \mathbf{q}', \sigma') \psi(\mathbf{k} + \mathbf{q}', \sigma'), \quad (2)$$

with  $\mathbf{k} \in \mathcal{B}$ ,  $\mathbf{q} \in \Lambda$ , where  $\mathcal{B}$  is the Brillouin zone of  $\Lambda$ , and  $\rho_{\mathbf{k}}$  are positive matrices satisfying  $0 \leq \rho_{\mathbf{k}} \leq 1/N$ .

In the following, we concentrate on fully polarized (P) and unpolarized (U) states where  $\rho_{\mathbf{k}}$  is restricted to a two component vector,  $\text{Tr}\rho_{\mathbf{k}\uparrow} = \text{Tr}\rho_{\mathbf{k}\downarrow}$ , but  $\rho_{\mathbf{k}\uparrow}$  may differ from  $\rho_{\mathbf{k}\downarrow}$ . We have checked that the ground state is either U or P except close to the polarization transition (see Supplemental Material [13]). Without any specification,  $k_F = [6\pi^2 N a_B^3 / (n_s V)]^{1/3} = \alpha/r_s$ ,  $\alpha^3 = 9\pi/(2n_s)$ , denotes the Fermi wave vector according to the polarization of the corresponding state, with  $n_s = 2$  for U and  $n_s = 1$  for P. For FG solutions, we have  $\rho_{\mathbf{k},\sigma}(\mathbf{q}, \mathbf{q}') = \delta_{\mathbf{q}\mathbf{q}'} \Theta(k_F - \|\mathbf{k} + \mathbf{q}\|)/N$  and the energy per electron is  $E_{\text{FG}} = 3k_F^2/10 - 3k_F/(4\pi) = 3\alpha^2/(10r_s^2) - 3\alpha/(4\pi r_s)$  in hartree units.

On the other hand, in the Wigner crystal, each  $\rho_{\mathbf{k}}$  is  $1/N$  times a projector of rank  $n_s$ . This case has already been considered with various symmetries in Ref. [11], but their solutions did not lower the energy for  $r_s \leq 4.4$ , and a transition to the FG has been predicted.

Of course, the true ground state solutions are expected to be somewhere between the FG and WC solutions. Unrestricted HF calculations for small systems [12] ( $N < 10^3$ ) have indicated the possibility of a spin-density wave in this region with energy gains of order  $10^{-4}$  hartree with respect to FG. In fact, at small  $r_s$ , as the system goes to the FG, the crystalline order remains but the Brillouin zone becomes partially occupied. In particular, the number of particles per unit cell is not known *a priori*. The purpose of this Letter is to find these extremal periodic states without extra hypotheses for various lattice symmetries. In our notation, pure SDW are U states verifying  $\rho_{\mathbf{k}\uparrow}(\mathbf{q}; \mathbf{q}') = -\rho_{\mathbf{k}\downarrow}(\mathbf{q}; \mathbf{q}')$ , for  $\mathbf{q} \neq \mathbf{q}'$ .

Thus, we search for a lattice  $\Lambda$  and a density matrix  $\rho_{\mathbf{k}}$  such that the number of particles per unit cell is near  $n_s$  (or some multiple of  $n_s$  for non-Bravais lattices). Notice that for extremal states, the eigenvalues of  $\rho_{\mathbf{k}}$  must be exactly 0 or  $1/N$ . The number of strictly positive eigenvalues is not known *a priori*, but is expected to fall between 0 and  $2n_s$  (or some multiple of  $2n_s$  for non-Bravais lattices).

We truncate the number of vectors of the sublattice  $\Lambda$ , including only the first  $M_\Lambda$  bands:  $\rho_{\mathbf{k}}$  is a square matrix of order  $n_s M_\Lambda$ . The condition  $0 \leq \rho_{\mathbf{k}} \leq 1/N$  is difficult to fulfill, so we choose the representation

$$\rho_{\mathbf{k}} = \sum_i D_{\mathbf{k},i} |u_{\mathbf{k},i}\rangle \langle u_{\mathbf{k},i}|, \quad (3)$$

where  $\langle u_{\mathbf{k},i} | u_{\mathbf{k},j} \rangle = \delta_{ij}$  and  $0 \leq D_{\mathbf{k},i} \leq 1/N$ . Since the number of strictly positive  $D_{\mathbf{k},i}$  is between 0 and  $2n_s$ , we can restrict the summation in Eq. (3) over  $2n_s$  terms instead of  $n_s M_\Lambda$ . The number of unknowns is thus of order  $2n_s M_\Lambda$  times the number of vectors of  $\mathcal{B}$ . This is why we can deal with a large number of particles [17].

The minimization consists of the following steps. First, we choose  $D_{\mathbf{k},i}$  and  $|u_{\mathbf{k},i}\rangle$  to start with. Then, for  $D_{\mathbf{k},i}$  fixed, we find the best  $|u_{\mathbf{k},i}\rangle$  with a quadratic descent method

[14]. The next step is to try to improve  $D_{\mathbf{k},i}$  given the gradient of the energy with respect to  $D_{\mathbf{k},i}$  and the linear constraints  $0 \leq D_{\mathbf{k},i} \leq 1/N$  and  $\sum_{\mathbf{k},i} D_{\mathbf{k},i} = 1$ . We thus obtain a new set  $D_{\mathbf{k},i}^{(\text{new})}$  (either 0 or  $1/N$ ), and we change  $D_{\mathbf{k},i}$  into  $(1 - \varepsilon)D_{\mathbf{k},i} + \varepsilon D_{\mathbf{k},i}^{(\text{new})}$  (with a small enough  $\varepsilon$  to ensure that  $|u_{\mathbf{k},i}\rangle$  follows  $D_{\mathbf{k},i}$  *adiabatically*) and we restart the minimization with respect to  $|u_{\mathbf{k},i}\rangle$ . The process stops as soon as  $D_{\mathbf{k},i}^{(\text{new})} = D_{\mathbf{k},i}$ . In this case almost every  $D_{\mathbf{k},i}$  is 0 or  $1/N$  and the gradient is negative or positive accordingly.

The parameters are  $r_s$  (for the density), the lattice symmetry, the (smallest) modulus  $Q$  of the generators of  $\Lambda$ , the number  $M^3$  of points in the Brillouin zone  $\mathcal{B}$ , and the number  $M_\Lambda$  of plane waves per single-particle state.

*A priori*, we look for lattices with the lowest Madelung energies as they will lead to the more stable states at low densities. However, as the density increases, other lattices may become more favorable. Investigated lattices are simple cubic (sc), face-centered cubic (fcc), body centered cubic (bcc), and hexagonal (Hex) (see Table I).

For WC phases,  $Q = Q_W$ , whereas  $Q \neq Q_W$  characterizes incommensurate crystals, and  $Q \geq 2k_F$  leads to the FG solution with isotropic Fermi surface at  $k_F$ . Increasing  $M_\Lambda$  increases the basis resulting in a lower energy due to the variational principle. Our discretization of the Brillouin zone ranges from  $M = 32$  up to  $M = 128$ , which corresponds to effective system sizes with a number of electrons ( $\sim M^3$ ) much larger than those of Ref. [12].

Finite size effects are important in fermionic Coulomb systems [19] and, contrary to  $M_\Lambda$ , there is no variational principle. As the memory size increases  $\propto M_\Lambda^2 M^3$ , pure

TABLE I. The best overall ground states depending on  $r_s$  (last line). IC stands for incommensurate crystal, otherwise it is WC.  $n_m$  is the number of maxima of charge density per unit cell [18].  $T$  is the shift between the spin-up and -down lattices, in the conventional (Cartesian) cell basis for sc, fcc, and bcc lattices, and in the primitive cell basis for Hex and Hex<sup>(2)</sup> (number in parenthesis is the number of sites per cell).  $T_1 = (\frac{1}{3}, \frac{2}{3}, \frac{1}{2})$ ,  $T_2 = (\frac{1}{2}, 0, \frac{1}{4})$ . The asterisk means close to. The last line of each table indicates the range of  $r_s$  where each phase may be in the ground state.

		Unpolarized			
Symmetry	IC bcc	Hex <sup>(2)</sup> (hcp*)	fcc	sc	Hex
$n_m$	2	4	2	2	2
Charge	IC bcc <sup>(2)</sup>	Hex <sup>(4)</sup>	sc	bcc	hcp
$T$	$(\frac{1}{2}, \frac{1}{4}, 0)$	$T_2$	$(\frac{1}{2}, 0, 0)$	$(\frac{1}{2}, \frac{1}{2}, \frac{1}{2})$	$T_1$
$r_s$	3–3.4	3.4–3.7	3.7–5.9	5.9–9.3	
		Polarized			
Symmetry	sc	Hex <sup>(2)</sup> (hcp)	fcc	bcc	
$n_m$	1	2	1	1	
$Q_W/k_F$	1.61	0.88	1.76	1.81	
$r_s$		9.3–10.3	10.3–13	13–	

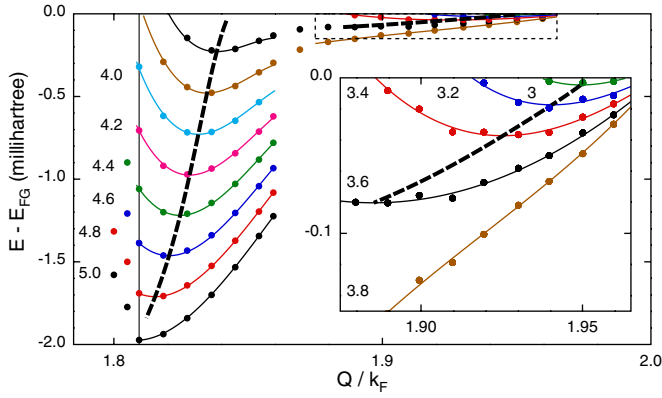


FIG. 1 (color online). Energy versus the modulation  $Q$  at various  $r_s$  for the unpolarized gas in the bcc symmetry. Lines come from a global polynomial fit on the numerical results (circles) of order 2 and 3 in  $r_s$  and  $Q$ , respectively.  $r_s$  is indicated at the start of each curve. Thick dashed lines go through the local minima. The leftmost vertical straight line stands for  $Q = Q_W$ . Inset: Enlargement of the dotted rectangle of the main figure.

numerical extrapolation to the thermodynamic limit ( $M \rightarrow \infty$ ) is difficult. Therefore, to accelerate convergence, we have included finite size corrections:

$$\Delta E_M \equiv E_M - E_\infty = E_M^{(1)} + E_M^{(2)} + E_{NA}, \quad (4)$$

where  $E_M^{(1)} \sim M^{-1}$  is the Madelung energy,  $E_M^{(2)}$  is an analytical potential energy error of order  $M^{-2}$ , and  $E_{NA}$  contains the nonanalytical energy corrections of order  $M^{-3}$ . From the FG potential energy,  $E_M^{(2)}$  can be estimated as

$$E_M^{(2)} = -\left(\frac{\gamma}{\pi M} \frac{S(\mathbf{k})}{\|\mathbf{k}\|} \Big|_{k \rightarrow 0}\right) E_M^{(1)}, \quad (5)$$

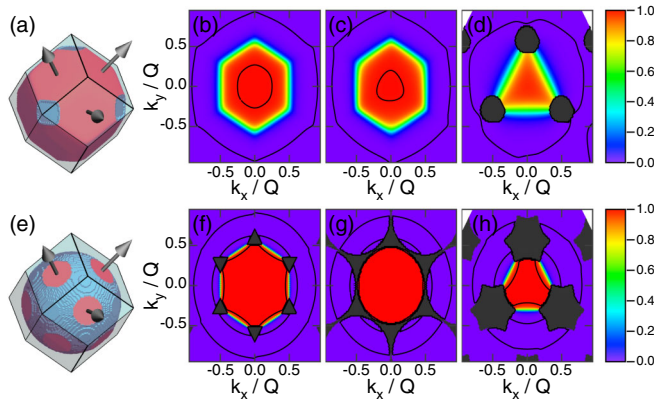


FIG. 2 (color online). Momentum distribution per spin  $n(\mathbf{k})$  for incommensurate solutions in bcc symmetry. (a) Iso surface at  $n(\mathbf{k}) = 0.5$  for  $Q/k_F \approx 1.827$ ,  $r_s = 4.2$ ,  $M = 64$ , and  $M_\Lambda = 19$ . The jump of  $n(\mathbf{k})$  from 0 to a nonzero value is shown in blue. Black arrows stand for reciprocal lattice vectors ( $\mathbf{Q}_1, \mathbf{Q}_2, \mathbf{Q}_3$ ). (b)–(d) Cut of  $n(\mathbf{k})$  in the plane ( $\mathbf{Q}_1, \mathbf{Q}_2$ ) at  $k_3 = 0$ ,  $Q/4$ , and  $Q/2$ , respectively. Black areas correspond to  $n(\mathbf{k}) = 0$ . Contour levels are at 0.99,  $10^{-3}$ , and  $10^{-5}$ . (e)–(h) Same as (a)–(d) for  $Q/k_F \approx 1.940$  and  $r_s = 3.2$ .

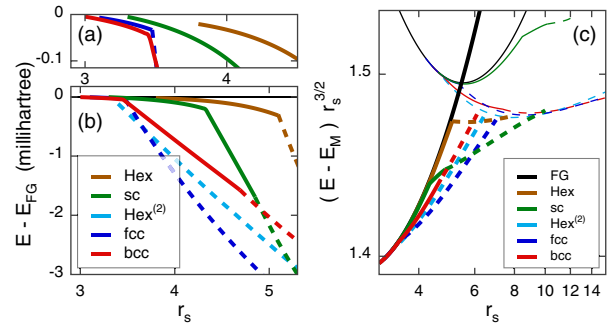


FIG. 3 (color online). Phase diagram of the electron gas: unpolarized (a),(b); polarized and unpolarized (c). Energies are in milihartrees for (a) and (b), and in hartrees for (c), where  $E_M = 0.89593/r_s$  is the Madelung energy of a polarized bcc Wigner crystal. Full lines stand for incommensurate regime ( $Q > Q_W$ ) and dashed lines for the Wigner crystal ( $Q = Q_W$ ). Colors refer to the lattice (see Table I). (a) Enlargement of (b) around  $E - E_{FG} = 0$ . (c) Thin lines stand for the polarized gas (upper curves) and thick lines for the unpolarized gas [13].

where  $\gamma^3$  is the volume of  $\mathcal{B}$ , and  $S(\mathbf{k})$  is the structure factor [for FG,  $\lim_{k \rightarrow 0} S(\mathbf{k}) / \|\mathbf{k}\| = 3/(4k_F)$ ]. Note that  $E_M^{(2)}$  is maximum for FG, decreases with  $Q$  for incommensurate solutions, and vanishes for WC. As can be seen in Fig. 4, removing  $E_M^{(2)}$  greatly improves the thermodynamic limit extrapolation. However, the remaining nonanalytical contributions of order  $10^{-6}$  hartree become comparable to the energy gain at high densities and prevent a precise determination of the ground state for  $r_s \lesssim 3$ . Extending the analytical calculations of Ref. [20] from two to three dimensions, one can prove that the incommensurate phases are always energetically favorable for  $r_s \rightarrow 0$ .

The accuracy of our results is essentially controlled at large  $r_s$  by  $M_\Lambda$  ( $\rho_{\mathbf{k}}$  smooth but extended) and at small  $r_s$  by  $M$  ( $\rho_{\mathbf{k}}$  rapidly varying around  $k_F$ ). Figure 1 shows the energy differences  $\Delta E = E - E_{FG}$  versus the modulation

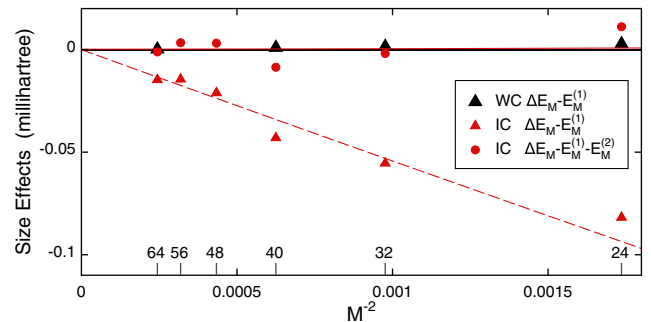


FIG. 4 (color online). Size effects on the potential energy for the U bcc lattice, Eqs. (4) and (5).  $E_M^{(i)}$  is the correction of order  $1/M^i$ . In red and black are the data for IC ( $r_s = 3.4$ ,  $Q/k_F = 1.92$ ) and WC [ $r_s = 5$ ], respectively. Red circles include second order correction for IC ( $E_M^{(2)} = 0$  for WC). The red dashed (full) line is a fit of the form  $E_M^{(2)} + b/M^3$  ( $b/M^3$ ). Numbers at the bottom indicate  $M$ .

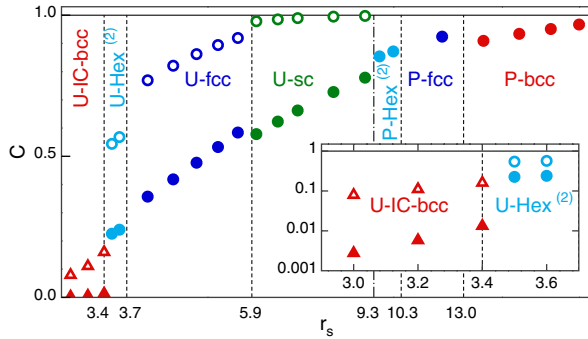


FIG. 5 (color online). Contrast  $C$  of  $n(\mathbf{r})$  versus  $r_s$  for the ground states. Full symbols: charge density. Open symbols (for unpolarized gas): spin-up (or -down) density. Circle: Wigner crystal. Triangle: Incommensurate phase (IC). Inset: Enlargement of the low- $r_s$  part. Vertical lines separate the different unpolarized (U) and polarized (P) phases. In the incommensurate phase, charge modulations are drastically reduced at higher densities and the solutions approach a pure SDW ground state.

$Q$  at various  $r_s$  for the U bcc symmetry. At large  $r_s$ , the minimum is found for  $Q = Q_W$ . At smaller  $r_s$ , a minimum is eventually reached for  $Q > Q_W$ . As seen in Fig. 1, two local minima may occur. Furthermore, at the local minima, the best solutions are always found with only one band [i.e., for each  $\mathbf{k} \in \mathcal{B}$  in Eq. (3), at most one  $D_{\mathbf{k},i}$  is nonzero].

The momentum distribution  $n(\mathbf{k})$  shows how the incommensurate states interpolate between the Wigner phase and the Fermi gas as  $r_s$  decreases ( $Q$  going from  $Q_W$  to  $2k_F$ ). For WC, the first band in  $\mathcal{B}$  is fully occupied and  $n(\mathbf{k})$  is everywhere continuous. At  $Q \gtrsim Q_W$ , the first band becomes partially filled and unoccupied volumes appear around the corners of  $\mathcal{B}$  [see Figs. 2(a)–2(d)], leading to a possible minimum at some  $Q_{\min}$ . Thus  $n(\mathbf{k})$  is discontinuous at the surface of these volumes but stay continuous in other directions. As  $Q$  increases, the volumes connect, allowing an eventual second minimum at  $Q \lesssim 2k_F$  [see Figs. 2(e)–2(g)]. At  $Q = 2k_F$ , the Fermi sphere is completed, where  $n(\mathbf{k})$  is discontinuous at the Fermi surface.

By construction, the real-space density  $n(\mathbf{r})$  has the crystalline symmetry of the lattice. In the incommensurate phase (IC), the number of maxima is greater than the number of electrons and depends on  $Q$ . At large  $r_s$ , the numbers coincide; this is the Wigner crystal. We define a contrast by  $C = (n^{\max} - n^{\min}) / (n^{\max} + n^{\min})$  which goes from 0 to 1 as  $r_s$  goes from 0 to infinity, where  $n^{\max}$  and  $n^{\min}$  are the maxima and minima of  $n(\mathbf{r})$ . For the unpolarized gas, we define the contrast for each spin species and for the total charge. As shown in Fig. 5, the contrast decreases rapidly as  $r_s$  goes to zero; it is expected [20] to be a nonanalytic function at  $r_s = 0$ . Note that the charge density modulation is much smaller than each spin modulation in the unpolarized gas demonstrating the SDW character of the ground state.

The final phase diagram of the unpolarized and polarized gas is reported in Fig. 3 and Table I. At high density, the incommensurate states have SDW character with modulations  $Q > Q_W$  which increase at smaller  $r_s$  towards  $Q = 2k_F$ . As only states close to the Fermi surface are relevant in this region, energy gains compared to FG become very tiny. Our resolution in  $k$  space is insufficient to determine the precise modulations for  $r_s < 3$ , which introduce small anisotropies in the Fermi surface for  $Q < 2k_F$ . Nevertheless, our calculations explicitly confirm the instability of the FG towards SDW [3,10] and indicate that the spin modulation continuously approaches  $Q = 2k_F$  with isotropic Fermi surface for  $r_s \rightarrow 0$ .

To conclude, we have established the true ground state phases of jellium within the Hartree-Fock approximation over a broad density region. In particular, we have shown that the Overhauser instability [10] of the FG results in a new ground state in the thermodynamic limit, characterized by an incommensurate crystal structure for the spin and charge density. However, it is known that the Hartree-Fock approximation tends to favor crystalline phases, as the gain in correlation energy is typically higher in the isotropic FG phase than in the WC [1]. Therefore, the transition to the WC is quantitatively incorrect within the HF approximation and shifted towards considerably higher values of  $r_s$  in the true ground state phase diagram. Whereas correlations certainly stabilize the FG at small  $r_s$ , correlations should favor incommensurate phases compared to WC for the same reason, so that incommensurate states should actually occur at densities close to crystallization. We hope that future QMC calculations will be able to establish this new phase beyond the HF approximation.

\*bernu@lptmc.jussieu.fr

- [1] D. M. Ceperley and B. J. Alder, *Phys. Rev. Lett.* **45**, 566 (1980).
- [2] B. Tanatar and D. M. Ceperley, *Phys. Rev. B* **39**, 5005 (1989).
- [3] G. F. Giuliani and G. Vignale, *Quantum Theory of the Electron Liquid* (Cambridge University Press, Cambridge, England, 2005).
- [4] E. P. Wigner, *Trans. Faraday Soc.* **34**, 678 (1938); *Phys. Rev.* **46**, 1002 (1934).
- [5] B. Bernu, L. Candido, and D. M. Ceperley, *Phys. Rev. Lett.* **86**, 870 (2001).
- [6] L. Cândido, B. Bernu, and D. M. Ceperley, *Phys. Rev. B* **70**, 094413 (2004).
- [7] M. Holzmann, B. Bernu, V. Olevano, R. M. Martin, and D. M. Ceperley, *Phys. Rev. B* **79**, 041308 (2009).
- [8] M. Holzmann, B. Bernu, C. Pierleoni, J. McMinis, D. M. Ceperley, V. Olevano, and L. Delle Site, *Phys. Rev. Lett.* **107**, 110402 (2011).
- [9] J. J. Shepherd, G. Booth, A. Grüneis, and A. Alavi, *Phys. Rev. B* **85**, 081103(R) (2012).
- [10] A. W. Overhauser, *Phys. Rev. Lett.* **4**, 462 (1960); *Phys. Rev.* **128**, 1437 (1962).

- [11] J. R. Trail, M. D. Towler, and R. J. Needs, *Phys. Rev. B* **68**, 045107 (2003).
- [12] S. Zhang and D. M. Ceperley, *Phys. Rev. Lett.* **100**, 236404 (2008).
- [13] See Supplemental Material at <http://link.aps.org/supplemental/10.1103/PhysRevLett.111.166402> for values of energies versus  $r_s$  and a detailed discussion of the polarization transition.
- [14] B. Bernu, F. Delyon, M. Duneau, and M. Holzmann, *Phys. Rev. B* **78**, 245110 (2008).
- [15] B. Bernu, F. Delyon, M. Holzmann, and L. Baguet, *Phys. Rev. B* **84**, 115115 (2011).
- [16] S. Huotari, J. A. Soininen, T. Pylkkänen, K. Hämäläinen, A. Issolah, A. Titov, J. McMinis, J. Kim, K. Esler, D. M. Ceperley, M. Holzmann, and V. Olevano, *Phys. Rev. Lett.* **105**, 086403 (2010).
- [17] This method needs less space memory and CPU times than that of Ref. [15].
- [18] For Wigner solutions,  $n_m$  is also the number of electrons per unit cell.
- [19] S. Chiesa, D. M. Ceperley, R. M. Martin, and M. Holzmann, *Phys. Rev. Lett.* **97**, 076404 (2006).
- [20] F. Delyon, M. Duneau, B. Bernu, and M. Holzmann, [arXiv:0807.0770](https://arxiv.org/abs/0807.0770).